Combined Crossed Molecular Beam and Theoretical Studies of the $N(^2D) + CH_4$ Reaction and Implications for Atmospheric Models of Titan†

Nadia Balucani,* Astrid Bergeat,‡ Laura Cartechini,§ Gian Gualberto Volpi, and Piergiorgio Casavecchia

Dipartimento di Chimica, Università degli Studi di Perugia, 06123 Perugia, Italy

Dimitris Skouteris

Dipartimento di Matematica e Informatica and Dipartimento di Chimica, Università degli Studi di Perugia, 06123 Perugia, Italy

Marzio Rosi

Dipartimento di Ingegneria Civile e Ambientale and ISTM-CNR, c/o Dipartimento di Chimica, Università degli Studi di Perugia, 06123 Perugia, Italy

Received: May 8, 2009; Revised Manuscript Received: July 8, 2009

The dynamics of the H-displacement channel in the reaction $N(^2D) + CH_4$ has been investigated by the crossed molecular beam (CMB) technique with mass spectrometric detection and time-of-flight (TOF) analysis at five different collision energies (from 22.2 up to 65.1 kJ/mol). The CMB results have identified two distinct isomers as primary reaction products, methanimine and methylnitrene, the yield of which significantly varies with the total available energy. From the derived center-of-mass product angular and translational energy distributions the reaction micromechanisms, the product energy partitioning and the relative branching ratios of the competing reaction channels leading to the two isomers have been obtained. The interpretation of the scattering results is assisted by new ab initio electronic structure calculations of stationary points and product energetics for the CH_4N ground state doublet potential energy surface. Differently from previous theoretical studies, both insertion and H-abstraction pathways have been found to be barrierless at all levels of theory employed in this work. A comparison between experimental results on the two isomer branching ratio and RRKM estimates, based on the new electronic structure calculations, confirms the highly nonstatistical nature of the $N(^2D) + CH_4$ reaction, with the production of the CH_3N isomer dominated by dynamical effects. The implications for the chemical models of the atmosphere of Titan are discussed.

1. Introduction

Chemical reactions involving atomic nitrogen are of relevance in a variety of natural environments, such as the upper terrestrial atmosphere[1] and the atmospheres of other planets,[2] and applied processes, where molecular nitrogen is deliberately introduced or present because it is the main component of air. Notable examples are plasma-induced chemical vapor deposition of nitrogen-doped diamond[3] and metal nitrocarburizing[4] using afterglow plasma or combustion in air.[5] Although kinetic studies are available[1,5] and reaction mechanisms have been speculated from rate constants, a better knowledge of the reactive behavior of atomic nitrogen requires an investigation at the level of reaction dynamics. The capability achieved in our laboratory to generate intense continuous supersonic beams of atomic nitrogen[6] has opened up the possibility of studying the reactive scattering of this species in crossed molecular beam (CMB) experiments with mass-spectrometric (MS) detection.[7−12]

In recent years, we have investigated[7−12] several reactions of N atoms in their first excited metastable state, $^2D_{5/2,3/2}$ (energy content: 230.0 kJ/mol; radiative lifetimes of $^2D_{3/2}$ and $^2D_{5/2}$ are 6.1×10^4 and 1.4×10^5 s, respectively[13]). Notwithstanding its high energy content, the metastable character of $N(^2D)$ and the much larger rate constants of its reactions with respect to those of $N(^4S)$[13,14] (especially when the reactive partner is a closed-shell molecule) suggest a potential role of this species in the above-mentioned chemical environments, similarly to the case of $O(^1D)$ as opposed to $O(^3P)$. For instance, the presence of $N(^2D)$ in the flame front has been invoked to explain chemi-ionization in ammonia/oxygen flames.[15] $N(^2D)$ was found to be the main product of the combustion reaction $O(^3P) + CN$[16] and similar chemical production of $N(^2D)$ can probably occur to a significant extent in combustion and plasma systems since few reactants adiabatically correlate with the quartet state. For instance, the initiation chain reaction of the prompt NO mechanism, $CH + N_2 \rightarrow HCN + N$, can form $N(^4S)$ only through a doublet-quartet intersystem-crossing (ISC),[17] which was found to have a low probability,[18] while the same reactants adiabatically correlate with $N(^2D)$. In particular, the reactions of $N(^2D)$ with simple hydrocarbons can be relevant in several discharge-induced processes, especially in chemical vapor deposition of nitrogen-doped diamond starting from N_2/CH_4 mixtures,[3] and in the chemistry of nitrogen dominated planetary

† Part of the special section "Chemistry: Titan Atmosphere".

* Corresponding author. Tel.: +39 075 585 5513. Fax: +39 075 585 5606. E-mail: nadia.balucani@unipg.it.

‡ Present address: Institut des Sciences Moléculaires, Université Bordeaux 1, 33405 Talence Cedex, France.

§ Present address: ISTM-CNR, c/o Dipartimento di Chimica, Università degli Studi di Perugia, 06123 Perugia, Italy.

10.1021/jp904302g CCC: $40.75
Published on Web 07/30/2009

atmospheres, such as that of Titan where a significant presence of methane and other hydrocarbons has been established.[19−24]

We have already reported on the investigation of the reaction dynamics of $N(^2D)$ with the unsaturated hydrocarbons acetylene[7] and ethylene.[8] For the two systems, we have been able to establish the main reaction primary products, that is, cyanomethylene and its cyclic isomer in the case of the $N(^2D) + C_2H_2$ reaction[7] and 2*H*-azirine and ketenimine in the case of the $N(^2D) + C_2H_4$ reaction.[8] For both reactions, the micromechanism involves the formation of bound intermediates, initially formed by the addition of the electrophilic $N(^2D)$ to the π cloud of the unsaturated hydrocarbon. We have also studied the reaction $N(^2D) + H_2(D_2) \rightarrow NH(ND) + H(D)$,[10,11] one of the few simple triatomic reactions for which accurate quantum dynamical calculations are available.[10] In this case, the reaction mechanism is quite different, being dominated by the insertion of $N(^2D)$ into the σ bond of molecular hydrogen.

Here we present an extension of the experimental investigation of another $N(^2D)$ reaction, that is the reaction $N(^2D) + CH_4(^1A_1)$. The thermodynamically allowed channels are

$$N(^2D) + CH_4(^1A_1) \rightarrow CH_2NH(^1A') + H(^2S) \quad \Delta H_0^0 = -321.2 \text{ kJ/mol} \quad (1a)$$

$$\rightarrow CHNH_2(^1A') + H(^2S) \quad \Delta H_0^0 = -172.0 \text{ kJ/mol} \quad (1b)$$

$$\rightarrow NH(^3\Sigma^-) + CH_3(^2A_2'') \quad \Delta H_0^0 = -126.1 \text{ kJ/mol} \quad (1c)$$

$$\rightarrow CH_3N(^3A_2) + H(^2S) \quad \Delta H_0^0 = -94.5 \text{ kJ/mol} \quad (1d)$$

$$\rightarrow NH_2(^2B_1) + CH_2(^3B_1) \quad \Delta H_0^0 = -54.6 \text{ kJ/mol} \quad (1e)$$

$$\rightarrow CH_2NH(^3A'') + H(^2S) \quad \Delta H_0^0 = -43.7 \text{ kJ/mol} \quad (1f)$$

$$\rightarrow CHNH_2(^3A'') + H(^2S) \quad \Delta H_0^0 = -30.1 \text{ kJ/mol} \quad (1g)$$

$$\rightarrow NH_2(^2B_1) + CH_2(^1A_1) \quad \Delta H_0^0 = -16 \text{ kJ/mol} \quad (1h)$$

where the enthalpies of reactions reported are those calculated in the present work (see below).

Previous studies have allowed to determine the rate constants at room temperature[25−27] and in the range 223−298 K[28] (the recommended[14] room temperature rate constant is 4.0×10^{-12} cm^3 $molecule^{-1}$ s^{-1}). The nascent rovibrational distributions of NH/ND products from the $N(^2D) + CH_4/CD_4$ reactions have been characterized in laser-induced-fluorescence experiments by Umemoto et al.,[29] who concluded that the NH product is formed by an insertion mechanism rather than abstraction, because of the similarity with the analogous reaction $O(^1D) + CH_4$. In a successive spectroscopic study,[30] Umemoto et al. also furnished the absolute yield of NH and H products, which were determined to be 0.3 ± 0.1 and 0.8 ± 0.2, respectively. Among the three possible H-displacement channels (leading to methanimine, CH_2NH, aminomethylidene, $CHNH_2$, and methylnitrene, CH_3N) the authors suggested channel 1a to be the dominant one on the basis of the energy release derived from H/D Doppler profile measurements which imply an average translational energy of ~80 kJ/mol. Some theoretical work is also available on reaction 1a, including ab initio calculations of the lowest CH_4N doublet potential energy surface (PES)[31−33] at different levels of theory and partial direct ab initio classical trajectory calculations.[34] There is no consensus on the favorite reaction approach: Takayanagi and co-workers[31,32,34] have derived an entrance barrier for both $N(^2D)$ insertion and direct H-abstraction, with the former being lower than the latter; the calculations by Jursic, instead, have provided a lower barrier for the H-abstraction mechanism.[33]

In our laboratory, we have performed a systematic study of the $N(^2D) + CH_4$ reaction as a function of collision energy by means of the CMB technique. One of the aims of our study is to elucidate whether the channel leading to $CH_2NH + H$ is the only active H-displacement pathway, as suggested by Umemoto et al.[30] Preliminary results obtained at a collision energy (E_c) of 37.2 kJ/mol have already been published[9] and the consequent implications for the atmospheric chemistry of Titan and prebiotic chemistry commented on.[12,35] Here we give a complete report of the experimental results at four other collision energies, with also a partial reanalysis of the published data at 37.2 kJ/mol. To clarify whether the favorite reaction mechanism is insertion or H-abstraction, the CMB-MS results are accompanied by new theoretical calculations of the stationary points of the relevant CH_4N potential energy surface (PES) at the B3LYP and CCSD(T) levels of theory, with thermochemical calculations also performed at the W1 level. RRKM estimates of the product branching ratios (BR) using the newly developed PES have also been performed and compared with our and previous BR results.[30,31] The importance of this reactive system for the chemistry of the atmospheres of Titan and solar planets will also be assessed.

2. Experimental Section

The scattering experiments were carried out by using a crossed molecular beam apparatus that has been described in detail elsewhere.[36] Briefly, two well-collimated, in angle and velocity, continuous supersonic beams of the reactants are crossed at 90° in a large scattering chamber with background pressure in the 10^{-7} mbar range, which assures the single collision conditions. The detection system consists of an electron impact ionizer, a quadrupole mass filter and an off-axis (90°) secondary electron multiplier. The ionizer is located in the innermost region of a triply differentially pumped ultrahigh-vacuum chamber, which is maintained in the 10^{-11} mbar pressure range in operating conditions by extensive turbo- and cryopumping. The whole detector unit can be rotated in the collision plane around an axis passing through the collision center and the velocities of the particles can be derived from time-of-flight (TOF) measurements.

The study of reaction 1a has been possible following the development in our laboratory of a continuous supersonic beam of nitrogen atoms containing, in addition to the electronic ground state ^4S, a sizable amount of the excited, metastable state ^2D. Atomic nitrogen beams have been generated by the high-pressure radio frequency discharge beam source successfully used in our laboratory over a number of years to generate intense supersonic beams of atoms and radicals.[6,36,37] In the present series of experiments, we have used a 0.23 mm diameter quartz nozzle and a boron nitride skimmer (diameter 0.9 mm) located

TABLE 1: Beam Characteristics at the Five Collision Energies Investigated (p = Stagnation Pressure, P_{nom} = Nominal RF Power, v = Beam Velocity, SR = Beam Speed Ratio, T_{nom} = Temperature)[a]

N beams					CH_4 beam					
gas mixture	p (mbar)	P_{nom} (W)	v (m/s)	SR	gas mixture	p (bar)	T_{nom} (K)	v (m/s)	SR	E_c (kJ/mol)
N_2(2%)/He(29%)/Ne	225	310	1945	7.2	pure CH_4	4.25	540	1469	7.1	22.2
N_2(2.5%)/He	240	310	2607	5.7	pure CH_4	2.5	300	1083	7.1	29.7
N_2(2.5%)/He	245	310	2646	8.2	pure CH_4	3.75	660	1683	6.8	37.2
N_2(2.5%)/He	280	315	2766	8.6	CH_4(25%)/H_2	3.25	295	2189	11.2	46.4
N_2(2.5%)/He	230	310	2728	8.2	CH_4(5.5%)/H_2	3.25	660	3161	14.3	65.1

[a] See text for details.

at a distance of 5.5 mm from the nozzle. The beam was further collimated by a rectangular slit to an angular divergence of 2.3°. Starting from a mixtures of N_2 (2.5%) in He or a mixture N_2(2%)/He(29%)/Ne, a high degree of molecular dissociation (~60%) was achieved. Atomic nitrogen was produced in a distribution of electronic states which has been characterized by Stern−Gerlach magnetic analysis:[6] 72% of the N atoms were found in the ground ^4S state, and 21% and 7%, in the metastable excited ^2D and ^2P states (the latter lying 343.5 kJ/mol above the ground state[13]). The use of nitrogen atom beams that contain also N(^4S) and N(^2P) does not represent a complication in the present experiments because the rate constant for the N(^4S) reaction is unmeasurably small[38] while the N(^2P) decay rate constant is smaller[28,39] than that for N(^2D) by a factor of 40−60 and is believed to be due essentially to physical quenching.[39]

In these experiments, different carrier gas mixtures and RF discharge operating conditions were used to achieve different beam velocities. The beam conditions and parameters of the nitrogen beams used in the present experiments are listed in Table 1.

The beams of CH_4 were produced by supersonic expansion through a 70 μm stainless-steel nozzle of pure CH_4 (stagnation pressure varied from 2.5 to 4.25 bar) or a mixture of CH_4/H_2 to increase the beam velocity. To vary the beam translational energy, the nozzle was also resistively heated in some experiments. The nominal temperature was read by a thermocouple placed close to the tip of the nozzle. Beam conditions and the relative peak velocities and speed ratios are also listed in Table 1. The beams were skimmed by a 1 mm stainless-steel skimmer and the beam angular divergence was about 6°.

The resulting five collision energies at which reactive scattering measurements have been performed are listed in Table 1. In addition to those experiments, to verify that the heating of CH_4 does not affect the reaction mechanism, we have repeated the experiment at 37.2 kJ/mol by using the same N beam and a room temperature beam of a mixture of CH_4 and H_2 in such a percentage (17%) that it had the same speed as that of pure CH_4 beam at 660 K. The two sets of measurements were identical within the experimental uncertainty, so implying that the heating of methane and the possible vibrational excitation do not significantly affect the reactive scattering distributions.

Reaction products could be detected at mass-to-charge ratios, m/z, of 29 (CH_3N^+) and 27 (CHN^+), while we could not operate at $m/z = 28$ because of the high inherent background signal at this mass-to-charge ratio and a strong interference from the undissociated N_2 coming from the nitrogen beam. The reactive scattering signal at $m/z = 29$ was also very noisy (probably because the quadrupole could not filter completely the contiguous very intense $m/z = 28$ signal) and affected by the undissociated N_2 from the beam containing one atom of the ^{15}N isotope. As a matter of fact, we only recorded the $m/z = 29$ angular distribution at two collision energies (37.2 and 46.4 kJ/mol) and verified that the $m/z = 27$ and $m/z = 29$ distributions were superimposable within the experimental error bars. This indicates that the signals recorded at $m/z = 27$ and $m/z = 29$ are due to the daughter HCN^+ and parent CH_3N^+ ions formed in the electron impact ionizer from the same neutral parent molecule(s) with gross formula CH_3N. Because of the better signal-to-noise ratio, all the final measurements were carried out at $m/z = 27$. The $m/z = 27$ laboratory angular distributions, $N(\Theta)$, were obtained by taking at least six scans of 50 s counts at each angle. An attempt to detect products from channel 1c failed, as both NH and CH_3 products are characterized by a parent ion at $m/z = 15$ where a strong interfering signal was caused by both the atomic nitrogen (through the isotope ^{15}N) and methane (through dissociative ionization to CH_3^+) beams.

The nominal angular resolution of the detector for a point collision zone is 1°. The secondary target beam (CH_4 beam) was modulated at 160 Hz with a tuning fork chopper for background subtraction. Velocity analysis of the beams was carried out by conventional "single-shot" time-of-flight (TOF) techniques, using a high-speed multichannel scaler and a CAMAC data acquisition system controlled by a personal computer. Velocity distributions of the products were obtained at selected different angles using the cross-correlation TOF technique with four 127-bit pseudorandom sequences. High-time resolution was achieved by spinning the TOF disk, located at the entrance of the detector, at 393.7 Hz corresponding to a dwell time of 5 μs/channel. The flight length was 23.6 cm. Counting times varied from 30 to 160 min depending upon signal intensity.

The scattering measurements have been carried out in the laboratory (LAB) system of coordinates, while for the physical interpretation of the scattering process it is necessary to transform the data (angular, $N(\Theta)$, and time-of-flight, $N(\Theta,t)$ distributions) to a coordinate system which moves with the center-of-mass (CM) of the colliding system. Because of the finite resolution of experimental conditions, i.e., finite angular and velocity spread of the reactant beams and angular resolution of the detector, the LAB-CM transformation is not single-valued, and therefore, analysis of the laboratory data is carried out by the usual forward convolution procedure, i.e., trial CM angular and velocity distributions are assumed, averaged and transformed to the LAB for comparison with the experimental data until the best fit of the LAB distributions is achieved.

3. Computational Details

The potential energy surface of the system N(^2D) + CH_4 was investigated by locating the lowest stationary points at the B3LYP[40] level of theory in conjunction with the correlation consistent valence polarized set aug-cc-pVTZ.[41] At the same level of theory we have computed the harmonic vibrational frequencies to check the nature of the stationary points, i.e.,

minimum if all the frequencies are real, saddle point if there is one, and only one, imaginary frequency. The assignment of the saddle points was performed using intrinsic reaction coordinate (IRC) calculations.[42] Finally, the energy of all the stationary points was computed at the higher level of calculation CCSD(T)[43] using the same basis set aug-cc-pVTZ. Both the B3LYP and the CCSD(T) energies were corrected to 0 K by adding the zero point energy correction computed using the scaled harmonic vibrational frequencies evaluated at B3LYP/aug-cc-pVTZ level. The energy of $N(^2D)$ was estimated by adding the experimental[13] separation $N(^4S)-N(^2D)$ of 230.0 kJ/mol to the energy of $N(^4S)$ at all levels of calculation. Thermochemical calculations were performed at the W1 level[44] of theory. All calculations were performed using Gaussian 03[45] while the analysis of the vibrational frequencies was performed using Molekel.[46]

4. RRKM Calculations

We have performed RRKM calculations on the $N(^2D) + CH_4$ system, using a code developed for this purpose. In accordance with the RRKM scheme,[47] the microcanonical rate constant for a specific reaction at a specific total energy (hereby denoted by $k(E)$) is given by the expression

$$k(E) = \frac{N_{TS}(E)}{\rho_r(E)}$$

where $N_{TS}(E)$ stands for the number of states (orthogonal to the reaction coordinate) open at the transition state at an energy E, and $\rho_r(E)$ denotes the reactant density of states at the same energy. Regarding the total angular momentum (J), the system was assumed to be described by a distribution of J states between 0 and 30, where each value of J is weighted by a factor proportional to its corresponding density of states at the energy concerned. We have noted that, even though the J distribution can influence considerably the absolute value of the rate constants, it only has a minimal effect on the BR.

The rotational densities of states, both for the reactants and for the transition states, were calculated using an inverse Laplace transform of the corresponding partition functions. Subsequently, the rotational densities of states were convoluted with the corresponding vibrational ones using a direct count algorithm. Finally, the density of states for the transition state was appropriately integrated with respect to the energy to produce the sum of states required. Given the high energies used with respect to all transition states, no tunneling contributions were included.

In the cases of "loose" transition states (monotonic dissociation channels), we performed ab initio and RRKM calculations at various points along the reaction coordinate, choosing as a transition state the point yielding the minimum value of the rate constant in accordance with the variational (VTST) approach. However, for the present system, spurious barriers were noted near the exit channels of some dissociation processes, which were due to interference of the first excited doublet electronic state. With this in mind, we have also performed calculations where the transition state was assumed to be the products at infinite separation.

5. Results and Analysis of Reactive Scattering Experiments

In Figures 1−5 are shown the $m/z = 27$ angular distributions in the LAB system obtained at the collision energies $E_{c1} = 22.2$ kJ/mol, $E_{c2} = 29.7$ kJ/mol, $E_{c3} = 37.2$ kJ/mol, $E_{c4} = 46.4$ kJ/mol and $E_{c5} = 65.1$ kJ/mol with the corresponding Newton diagrams. The error bars (representing ±1 standard deviation) are also reported when they exceed the size of the dots indicating the intensity averaged over the different scans. In the Newton diagrams of Figures 1−5 are also shown the Newton circles relative to the three possible isomers CH_3N (channel 1d, dashed lines), $CHNH_2$ (channel 1b, dashed-dotted lines), and CH_2NH (channel 1a, dotted lines) in the assumption that all the available energy is converted into product translational energy. The Newton circles delimit the LAB angular range within which each specific isomer can be scattered. The quite different exothermicity of the three channels imply a different extension of the Newton circles and of the relative scattering angular ranges.

TOF spectra at $m/z = 27$ were measured at selected LAB angles at $E_{c2} = 29.7$ kJ/mol, $E_{c3} = 37.2$ kJ/mol, and $E_{c4} = 46.4$ kJ/mol (see Figure 6−8), while no TOF spectra were recorded

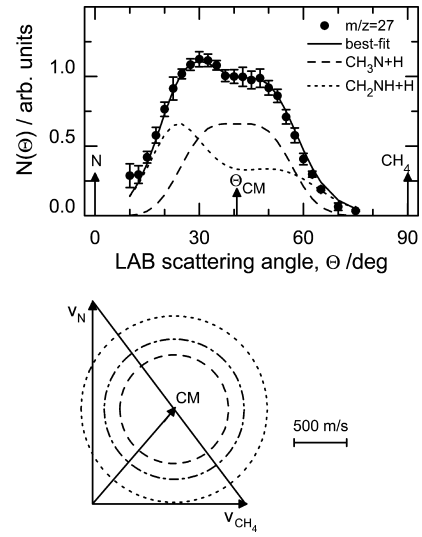

Figure 1. Laboratory angular distributions recorded at $m/z = 27$ for the reaction $N(^2D) + CH_4$ at $E_c = 22.2$ kJ/mol. Error bars, when visible outside the dots, represent ±1 standard deviation from the mean. The circles in the Newton diagram delimit the maximum velocity that the CH_2NH (dotted), $CHNH_2$ (dashed-dotted), and CH_3N (dotted) products from channels 1a, 1b, and 1d, respectively, can attain if all the available energy is channeled into product translational energy. The solid line is the total $N(\Theta)$ calculated when using the best-fit CM angular and translational energy distributions of Figure 9; the separated contributions of channel 1a (dotted line) and channel 1b and 1d (dashed line) are also indicated.

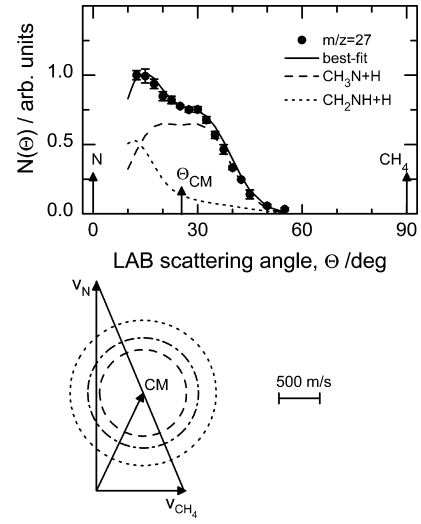

Figure 2. Same as Figure 1, but at $E_c = 29.7$ kJ/mol.

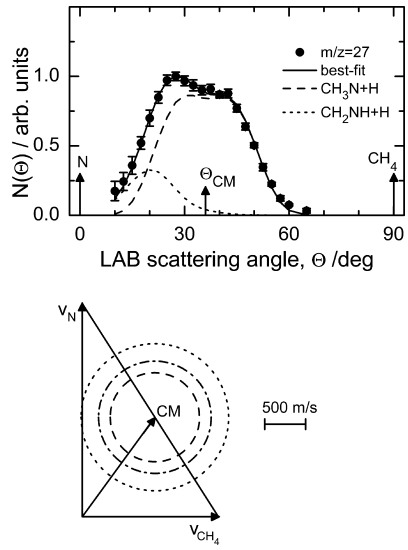

Figure 3. Same as Figure 1, but at $E_c = 37.2$ kJ/mol.

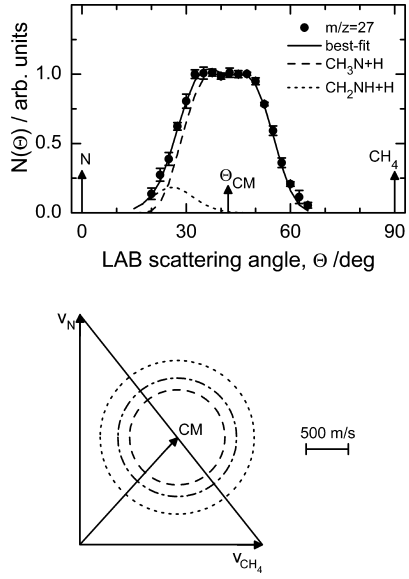

Figure 4. Same as Figure 1, but at $E_c = 46.4$ kJ/mol.

at $E_{c1} = 22.2$ kJ/mol and $E_{c5} = 65.1$ kJ/mol because of the lower signal-to-noise ratio of these sets of data (~30 as opposed to ~70−80 of the other experiments).

At first view, the LAB angular distributions reported in Figures 1−5 appear to be quite different, but such a difference is largely related to the different kinematics of the five experiments. Particularly, the acceleration of the CH_4 beam, achieved either by heating the pure gas or by using a CH_4/H_2 mixture, drastically modifies the kinematics of the experiments and hence the position of the center-of-mass velocity vector, the extent of the Newton circles and the width of the angular distributions. In spite of the apparent differences, the angular distributions share substantial similarities. In all cases the product flux is distributed on both sides of the CM angle, Θ_{CM}. This feature by itself might suggest that the reaction mechanism is dominated by the formation of bound intermediates. The LAB angular distributions recorded at E_{c1} and E_{c2} exhibit a clear preference for forward scattering, which diminishes with the increase of E_c until it disappears at the highest collision energy investigated. Also, if one refers to the extent of the Newton circles of each experiments, it can be noted that the width of the angular distributions is more in line with the most exothermic

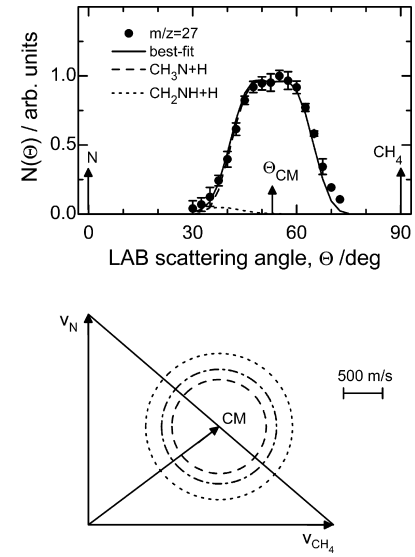

Figure 5. Same as Figure 1, but at $E_c = 65.1$ kJ/mol.

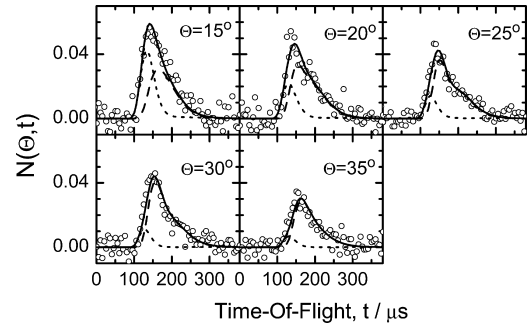

Figure 6. Time-of-flight distributions of the CH_3N products (open circles) detected at $m/z = 27$ for the reaction $N(^2D) + CH_4$ at $E_c = 29.7$ kJ/mol at the indicated LAB angles. Solid lines represent the TOF distributions calculated from the best-fit CM functions reported in Figure 9. The separated contributions of channel (1a) (dotted lines) and channel (1b)/(1d) (dashed lines) are also indicated.

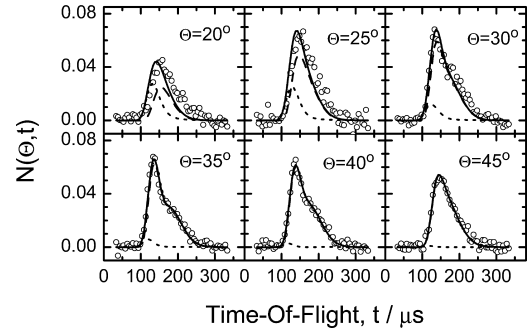

Figure 7. Same as Figure 6, but at $E_c = 37.2$ kJ/mol.

channel 1a at the low collision energy of 22.2 kJ/mol, while it becomes progressively more in line with the least exothermic channel 1d with the increase of the collision energy. The observed trends imply that two different reaction mechanisms are at play, which can be attributed to at least two different reaction channels and the importance of which is varying with the available energy. In particular, the most exothermic channel predominates at the lowest collision energies and is characterized by some forward scattering preference, while the least exothermic channel dominates at the highest E_c investigated and is characterized by more isotropic angular distributions. Similar features are also reflected in the TOF data, where the TOF spectra recorded at angles smaller than Θ_{CM} have a fast

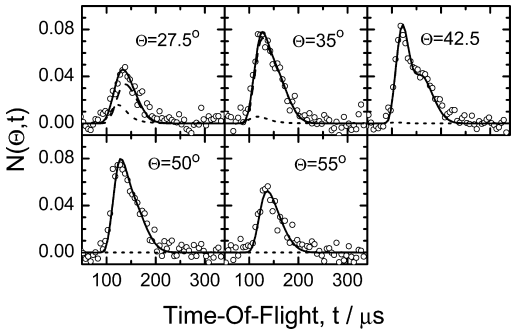

Figure 8. Same as Figure 6, but at E_c = 46.4 kJ/mol.

TABLE 2: Best Fit Relative Weights, $\alpha = w_1/w_2$, of the Two Contributions Associated with the $CH_3N/CHNH_2$ and CH_2NH Channels[a]

best-fit α values	uncertainty	E_c (kJ/mol)
1.33	±10%	22.2
0.8	±10%	29.7
0.25	±20%	37.2
0.1	±20%	46.4
0.03	±100%	65.1

[a] See text for details.

components which is absent for those recorded at the right of Θ_{CM} for the experiments at E_{c2} and E_{c3}, while they are essentially unimodal for the experiment at E_{c4}.

The presence of two contributions has been confirmed during the data analysis, as the fit of the LAB distributions could not be obtained unless two different sets of CM functions were used. In the forward convolution trial and error fitting procedure the CM product flux was expressed according to

$$I_{CM}(\theta, (E'_T)) = w_1 T(\theta)_1 P(E'_T)_1 + w_2 T(\theta)_2 P(E'_T)_2$$

where $T(\theta)_1$, $T(\theta)_2$ and $P(E'_T)_1$, $P(E'_T)_2$ are the CM angular and translational energy distributions associated, respectively, to the two contributions. The coefficients w_1 and w_2 are the relative weights of the two contributions and were treated as adjustable parameters during the fitting procedure. The best-fit w_2/w_1 values, indicated with the symbol α in the rest of the paper, are reported in Table 2. As can be seen, they vary significantly with E_c and the contribution of the more exothermic channel significantly decreases with increase of collision energy. According to the energetics of the reaction channels, the more exothermic contribution is clearly attributable to CH_2NH formation channel 1a, while the less exothermic contribution can be attributed to either the CH_3N or $CHNH_2$ formation channel. In Figures 1−8 the continuous curves represent the global best-fit of the experimental data, while the dashed and the dotted lines represent the contributions of the $CH_3N/CHNH_2$ + H and CH_2NH + H channels, respectively. The best-fit CM distributions are reported in Figure 9 (dotted lines refer to the CH_2NH channel, dashed line to the CH_3N + $H/CHNH_2$ + H channel).

The best-fit CM angular distributions associated to channel 1b and 1d are isotropic at all collision energies investigated. Slightly polarized backward−forward symmetric CM angular distributions still afford an acceptable fit of the experimental distributions. This feature is consistent with the formation of a bound intermediate. Also the best-fit product translational energy distributions associated to this channel exhibit about the same characteristics. The fit of both angular and TOF distributions was particularly sensitive to the rise and peak shape of $P(E'_T)$, while it was less sensitive to its

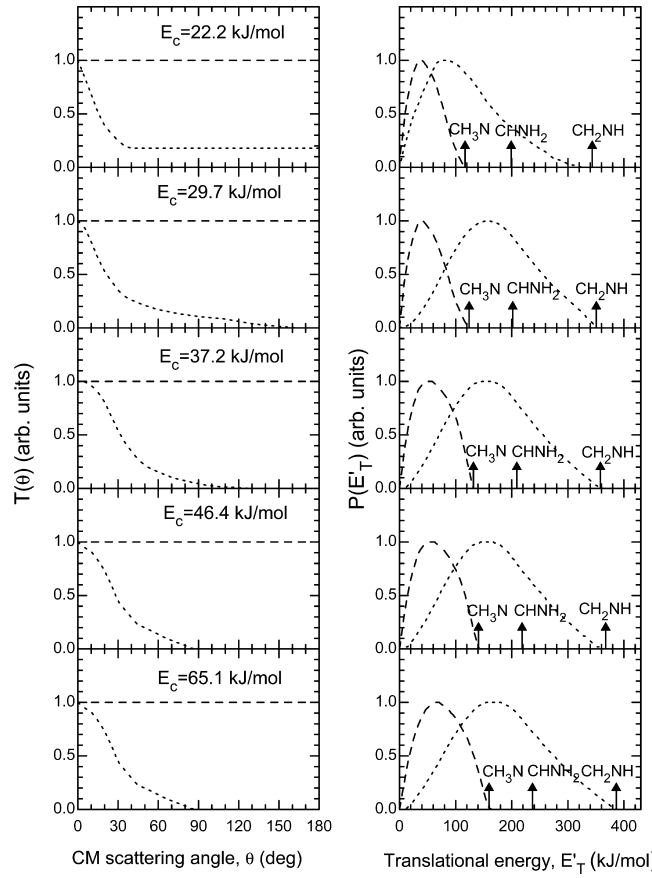

Figure 9. Best-fit CM product (left column) angular and (right column) translational energy distributions at the indicated collision energies. Dotted lines refer to channel (1a); dashed lines refer to channels (1b) and (1d). The arrows in the right panels indicate the total energy available to the products for the three channels leading to the isomers CH_3N, $CHNH_2$, and CH_2NH.

high energy cutoff. This is an important issue for the attribution of these sets of CM functions to channel 1b rather than 1d. All the best-fit $P(E'_T)$'s end within the maximum available energy of channel 1d, but we have performed some sensitivity tests and found that if we add a tail with an intensity less than 0.1 up to the maximum energy available for channel 1b, the fit of the experimental distributions is not particularly affected. Nevertheless, even though we cannot exclude that channel 1b contributes to some extent, the global shapes of the $P(E'_T)$s are more in line with the energetics of channel 1d. In the assumption that only channel 1d contributes, the average product translational energy, defined as $\langle E'_T \rangle = \Sigma P(E'_T)E'_T/\Sigma P(E'_T)$ corresponds to a fraction, f_T, of the total available energy ($E_{tot} = E_c - \Delta H°_0$, where the theoretical value of $\Delta H°_0 = -94.5$ kJ/mol is used) of 0.40 at E_{c1} and E_{c2}, which rises up to 0.47 at E_{c3}, E_{c4}, and E_{c5}.

The best-fit CM angular distributions derived for the CH_2NH channel are quite different, as they show a distinct preference for the forward hemisphere. Interestingly, the best-fit $T(\theta)$ at the lowest E_c has some intensity in the entire angular range and is characterized by a sharp peak at $\theta = 0°$. At E_{c2} the best-fit $T(\theta)$ has a tail extending up to 150° and the forward peak becomes more rounded. At E_{c3}, the tail extends only up to 110−120°, while at E_{c4} and E_{c5} the tails extend up to 90° and the forward peak is quite rounded. The sensitivity to the shape of the CM angular distribution is quite high for the low E_c experiments, where this contribution dominates or is quite important, while it is much lower at the highest E_c where the its importance becomes much smaller. As far as the best fit

$P(E'_T)$'s for the CH_2NH channel are concerned, they are quite similar for the experiments at $E_{c2} - E_{c5}$, while in the best-fit $P(E'_T)$ for the experiment at E_{c1} there is a shift in the peak position toward lower E'_T values. We recall, however, that at this low E_c we did not record TOF spectra because of the low signal-to-noise ratio, and therefore, the determination of the product CM translational energy distribution is affected by some uncertainty. The fraction, f_T, of the total available energy (where the theoretical value of $\Delta H°_0 = -321.2$ kJ/mol is used) is 0.34 at E_{c1} and 0.47 for the experiments at the other collision energies.

The best-fit α values reported in Table 2 are also affected by some uncertainty. They might vary by ±10% at the two lowest E_c investigated and ±20% at E_{c3} and E_{c4}. The sensitivity at the highest collision energy investigated is relatively small and the best-fit value of α can be varied by ±100%. The previously reported[9,12] best-fit value of α at 37.2 kJ/mol was affected by a numerical error in the determination of the relative weights. It should be noted that we have derived the relative importance of the two channels from the LAB scattering measurements at $m/z = 27$, that is from the distribution of the daughter ion HCN^+ originating from CH_2NH and $CH_3N/CHNH_2$ parent molecules. The fragmentation pattern of CH_2NH, CH_3N, and $CHNH_2$ are not known. Nevertheless, the observation that the $m/z = 27$ and 29 angular distributions are superimposable implies that the fraction of CH_2NH and $CH_3N/CHNH_2$ which ionize to HCN^+ in the ionizer is the same and that the branching ratios derived at $m/z = 27$ are representative of the BR of the neutral parent molecules.

6. Computational Results

The potential energy surface of $N(^2D) + CH_4$ has been investigated at the ab initio level. The lowest stationary points localized on this surface have been reported in Figure 10, where the main geometrical parameters (distances/Å and angles/deg) are shown together with the energies computed at B3LYP/aug-cc-pVTZ, CCSD(T)/ aug-cc-pVTZ and W1 level, relative to that of CH_2NH_2, which is the most stable isomer at all levels of calculation. The energy changes and barrier heights computed at 0 K with inclusion of the zero point energy correction for the main isomerization and dissociation processes are reported in Table 3, while a schematic representation of the potential energy surface of the $N(^2D) + CH_4$ system is shown in Figure 11. For the sake of simplicity in Figure 11 we have reported only the relative energies computed at the W1 level, while in Table 3 we have reported the values computed at all levels of calculation for comparison purposes. The total energies, the geometrical parameters, and the vibrational frequencies of all the stationary points (minima and saddle points) are provided as Supporting Information (Table S1). Many of the stationary points of interest in this work have been previously reported by Kurosaki et al.[31] and Jursic.[33] Kurosaki et al. optimized the geometries at MP2(full)/cc-pVTZ level of theory and computed the energies at PMP4(full,SDTQ)/cc-pVTZ level while Jursic performed mainly CBS-Q calculations. The products methylnitrene[48] and methanimine[49] have also been previously characterized at different levels of calculations. The agreement of our work with previous results is generally good, the differences being due to the different methods employed in this work.

In the following paragraph we will discuss our results; for simplicity we will refer only to the most accurate results, i.e., W1 results. The B3LYP and CCSD(T) values, however, are reported in Figure 10 and Table 3. From Figure 11 we can see that the interaction of $N(^2D)$ with CH_4 gives rise to the species CH_3NH, which is more stable than the reactants by 445.9 kJ/mol at W1 level. For this insertive approach we have found a saddle point that is, however, below the reactants at both B3LYP and CCSD(T) levels of calculation. We were not able to compute the energy of this point at the W1 level. The presence of saddle points below the reactants has already been observed for very exothermic reactions, in particular involving methane.[50] However, since we were not successful in localizing a stable initial complex, the energy of this saddle point does not seem to be very meaningful. We tried also to localize this saddle point at the MP2 level of calculations, but we did not succeed. Notably, this saddle point was computed at several levels of calculations by Takayanagi et al.[31,32] and their best estimate for the barrier height was calculated to be 5.3 kJ/mol above the reactants.[32] Such a barrier height, however, is still too high to account for the rate constant of reaction 1.[28] Once formed after $N(^2D)$ insertion into a C−H bond, CH_3NH either can isomerize to species CH_2NH_2, which is the most stable isomer of the NCH_4 PES, with a barrier of 152.6 kJ/mol or can directly dissociate to $CH_2NH(^1A')$ and H products through a slightly lower barrier of 137.0 kJ/mol. The other CH_3NH dissociation channels, i.e., those leading to $CH_3 + NH$ or $CH_3N + H$, are both barrierless, but they are very endothermic with respect to CH_3NH, the dissociation energies being 319.8 and 351.4 kJ/mol, respectively. In principle, CH_3N can be formed in either a triplet or a singlet state. According to the present calculations, however, only the triplet state is formed because singlet methylnitrene in its ground state rearranges without any barrier to methanimine. This is in agreement with previous experimental[51] and theoretical results.[52] Also, singlet methylnitrene (ã ^1E) is too high in energy ($\Delta E = 1.352 \pm 0.011$ eV)[51] to be produced in the conditions of the present experiment. The products $CH_3 + NH$ can also be reached directly from $N(^2D) + CH_4$ through a hydrogen abstraction process with a saddle point, which lies 76.6 kJ/mol

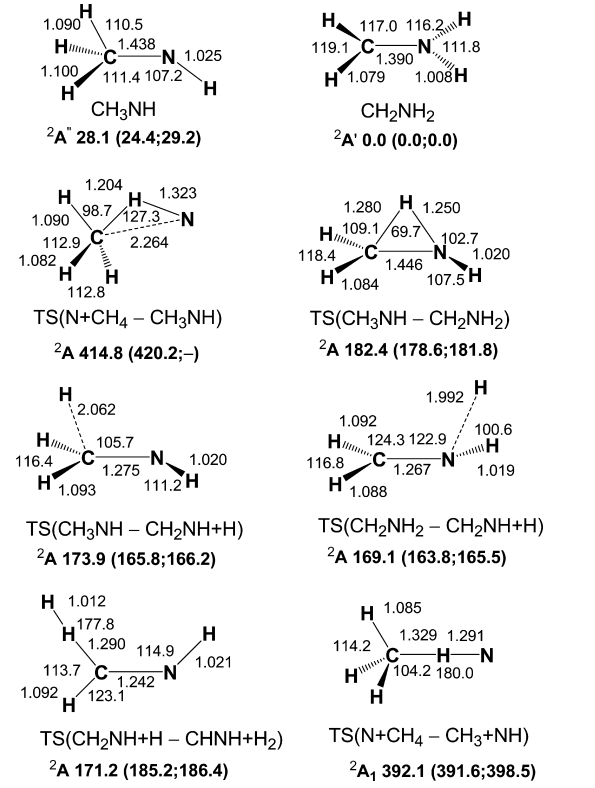

Figure 10. B3LYP optimized geometries (Å and deg) and relative energies (kJ/mol) at 0 K of minima and saddle points localized on the PES of $N(^2D) + CH_4$. CCSD(T) and W1 relative energies are reported in parentheses.

TABLE 3: Enthalpy Changes and Barrier Heights (kJ/mol, 0 K) Computed at the B3LYP/aug-cc-pVTZ, CCSD(T)/aug-cc-pVTZ, and W1 Levels of Theory for Selected Dissociation and Isomerization Processes for the System $N(^2D) + CH_4$

	$\Delta H°_0$			barrier height		
	B3LYP	CCSD(T)	W1	B3LYP	CCSD(T)	W1
$N(^2D) + CH_4 \rightarrow CH_3NH$	–466.0	–427.6	–445.9	–79.3	–31.8	–
$N(^2D) + CH_4 \rightarrow CH_3 + {}^3NH$	–153.2	–120.7	–126.1	–102.0	–60.4	–76.6
$CH_3NH \rightarrow CH_2NH_2$	–28.1	–24.4	–29.2	154.3	154.2	152.6
$CH_3NH \rightarrow {}^1CH_2NH + H$	136.9	126.6	124.7	145.8	141.4	137.0
$CH_3NH \rightarrow {}^3CH_2NH + H$	387.9	398.5	402.2			
$CH_3NH \rightarrow {}^3CH_3N + H$	345.7	343.0	351.4			
$CH_3NH \rightarrow CH_3 + {}^3NH$	312.8	306.9	319.8			
$CH_2NH_2 \rightarrow {}^1CH_2NH + H$	165.0	151.0	153.9	169.1	163.8	165.5
$CH_2NH_2 \rightarrow {}^3CH_2NH + H$	416.0	422.9	431.4			
$CH_2NH_2 \rightarrow {}^1CHNH_2 + H$	309.0	299.0	303.1			
$CH_2NH_2 \rightarrow {}^3CHNH_2 + H$	439.5	437.7	445.0			
$CH_2NH_2 \rightarrow {}^3CH_2 + NH_2$	413.1	404.5	420.5			
$CH_2NH_2 \rightarrow {}^1CH_2 + NH_2$	458.8	443.6	459.1			
$CH2NH + H \rightarrow CHNH + H_2$ H_2	–50.7	–34.7	–36.4	6.2	34.2	32.5

below the reactants. Also in this case we were not able to localize any stable initial complex. The geometry of this saddle point is comparable to that obtained by Jursic.[33] Once formed by CH_3NH isomerization, CH_2NH_2 can also lose an H atom, giving rise to the isomers $CH_2NH(^1A')$ (with an exit barrier of 165.5 kJ/mol) or $CHNH_2(^1A')$ (in a very endothermic, 303.1 kJ/mol, barrierless process). On energetic grounds, both CH_2NH and $CHNH_2$ can also be formed in their excited triplet states (channels 1f and 1g). Nevertheless, these excited states are formed adiabatically along the first excited doublet CH_4N PES, the entrance barrier of which has been found to be quite higher than that of the ground state doublet PES.[32] With the present methods of calculations, we are not able to derive the excited PESs and characterize the possible reactive channels along it. CH_2NH_2 can also dissociate into $CH_2(^3B_1,^1A_1) + NH_2$: these barrierless dissociation channels are endothermic by 420.5 and 459.1 kJ/mol for triplet and singlet CH_2 formation, respectively.

Finally, we have located a small barrier (32.5 kJ/mol) for the reaction of the CH_2NH product with its cofragment H to produce $CHNH + H_2$. This reaction is exothermic by 36.4 kJ/mol. The situation appears to be quite similar to that of the isoelectronic system $O + CH_3$, where the products H_2CO and H formed by the dissociation of the methoxy radical intermediate can interact further and produce $HCO + H_2$ in frustrated H loss trajectories.[53] Nevertheless, differently from the case of the $O + CH_3$ reaction for which indirect experimental evidence exists that $HCO + H_2$ are formed,[53] we did not gain any evidence that an H_2-loss channel is contributing to the measured distributions at $m/z = 27$.

7. RRKM Results

RRKM calculations have been carried out for eight values of the total energy (the zero of energy is assumed to be the reactants $N(^2D) + CH_4$ at infinite separation). Three of these (0.78, 1.65, and 1.45 kJ/mol) correspond to the surface temperature of Titan (94 K), to the stratospheric temperature of Titan (175 K), and to room temperature, while the other five

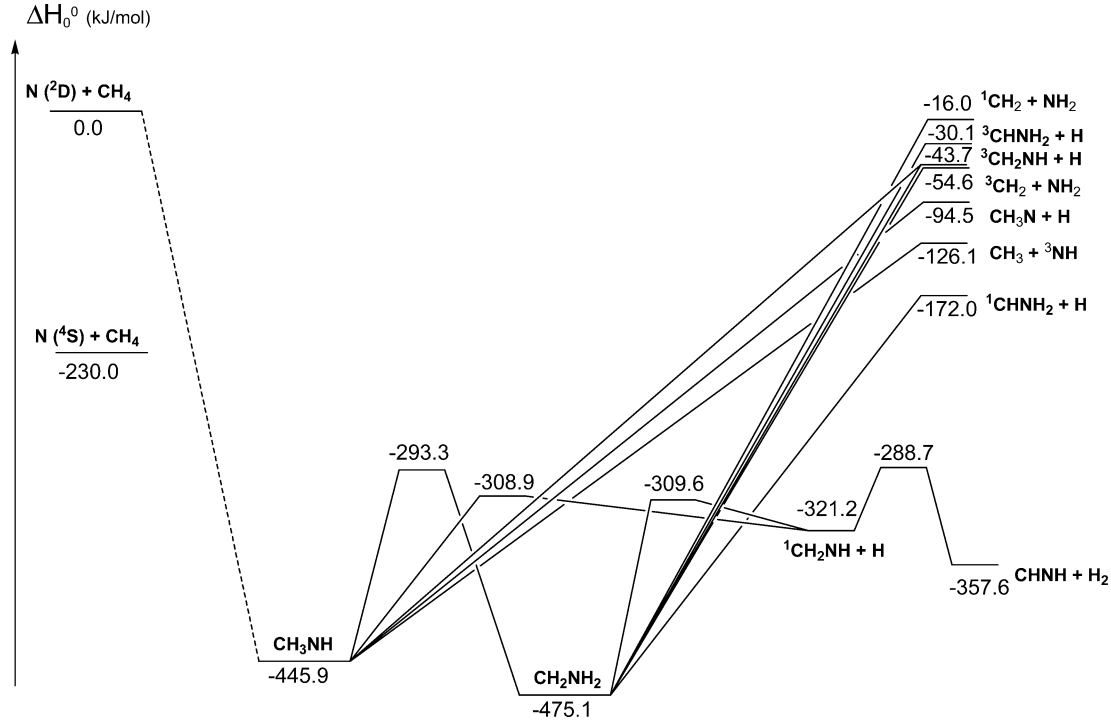

Figure 11. Schematic representation of the $N(^2D) + CH_4$ potential energy surface. For simplicity, only the W1 relative energies (kJ/mol) are reported.

TABLE 4: Microcanonical Rate Constants for Reaction Channels of the CH_3NH Intermediate, in Units of 1/s[a]

energy (kJ/mol)	CH_2NH_2	$CH_2NH + H$	$CH_3 + NH(A)$	$CH_3 + NH(D)$	$CH_3N + H(A)$	$CH_3N + H(D)$
0.78	4.26×10^{11}	4.28×10^{12}	1.38×10^{8}	3.09×10^{11}	1.57×10^{4}	6.38×10^{10}
1.45	4.28×10^{11}	4.30×10^{12}	1.44×10^{8}	3.13×10^{11}	2.10×10^{4}	6.53×10^{10}
2.49	4.32×10^{11}	4.34×10^{12}	1.53×10^{8}	3.20×10^{11}	2.68×10^{4}	6.75×10^{10}
22.2	5.03×10^{11}	5.07×10^{12}	4.52×10^{8}	4.68×10^{11}	6.11×10^{5}	1.23×10^{11}
29.7	5.32×10^{11}	5.36×10^{12}	6.46×10^{8}	5.33×10^{11}	1.38×10^{6}	1.51×10^{11}
37.2	5.61×10^{11}	5.66×10^{12}	9.02×10^{8}	6.04×10^{11}	2.89×10^{6}	1.83×10^{11}
46.4	5.98×10^{11}	6.03×10^{12}	1.32×10^{9}	6.98×10^{11}	6.32×10^{6}	2.30×10^{11}
65.1	6.76×10^{11}	6.82×10^{12}	2.63×10^{9}	9.15×10^{11}	2.40×10^{7}	3.51×10^{11}

[a] (A) and (D) denote, respectively, the adiabatic and the diabatic assumption (see text for details).

TABLE 5: Same as Table 4, for the Reactions of the CH_2NH_2 Intermediate

energy (kJ/mol)	CH_3NH	$CH_2NH + H$	$CHNH_2 + H$	$^3CH_2 + NH_2(A)$	$^3CH_2 + NH_2(D)$
0.78	2.16×10^{11}	3.66×10^{12}	7.00×10^{10}	2.01×10^{4}	1.76×10^{10}
1.45	2.17×10^{11}	3.69×10^{12}	7.09×10^{10}	2.35×10^{4}	1.81×10^{10}
2.49	2.19×10^{11}	3.72×10^{12}	7.21×10^{10}	3.39×10^{4}	1.88×10^{10}
22.2	2.60×10^{11}	4.40×10^{12}	9.97×10^{10}	2.06×10^{6}	3.90×10^{10}
29.7	2.77×10^{11}	4.68×10^{12}	1.12×10^{11}	5.37×10^{6}	4.98×10^{10}
37.2	2.94×10^{11}	4.96×10^{12}	1.25×10^{11}	1.20×10^{7}	6.26×10^{10}
46.4	3.16×10^{11}	5.32×10^{12}	1.43×10^{11}	2.79×10^{7}	8.11×10^{10}
65.1	3.63×10^{11}	6.08×10^{12}	1.83×10^{11}	1.13×10^{8}	1.30×10^{11}

(22.2, 29.7, 37.2, 46.4, and 65.1 kJ/mol) correspond to the collision energies used in the present CMB experiments.

According to the present PES calculations, the H-displacement channels are opened by $N(^2D)$ insertion into a C−H bond forming a CH_3NH intermediate. This intermediate, subsequently, can rearrange to form CH_2NH_2. All subsequent channels of the reaction proceed from one or both of these intermediates, and therefore, we have found it convenient to classify the rate constants according to the original intermediate.

In Table 4 are shown the rate constants for the reactions originating from CH_3NH. It can be seen that, at all energies, the dominant channel is dissociation into $CH_2NH + H$ followed by rearrangement into the second intermediate, CH_2NH_2. This result can be easily explained by the fact that the energy barriers for these processes are the lowest ones. As far as the other two channels are concerned, i.e., dissociation into $CH_3 + NH$ or $CH_3N + H$, we are faced with two possibilities. As mentioned earlier, the calculation of intermediate points along the reaction coordinate (for variational purposes) presents us with spurious barriers that are due to the avoided crossing between the ground and first excited doublet states. We have termed the results of these calculations as "adiabatic". On the other hand, the fact that spin−orbit coupling has not been taken into account in our calculations means that we are neglecting the possibility of crossing into the quartet manifold at the point of intersection (which lies in the product valley), thus avoiding the barrier. Hence, we have also performed RRKM calculations where the transition state has been assumed to lie at an infinite separation of the products. We have termed these results as "diabatic".

In the adiabatic case, both (1c) and (1d) channels are negligibly slow. The BR for rearrangement into CH_2NH_2 and dissociation into $CH_2NH + H$ are 0.09 and 0.91, respectively, at all energies. In the diabatic case, while the BR for rearrangement into CH_2NH_2 remains 0.08 at all energies, the BR for dissociation into $CH_2NH + H$ moves from 0.84 at the lowest energy to 0.81 at 37.2 kJ/mol up to 0.78 at 65.1 kJ/mol. At the same time, BRs for the $CH_3 + NH$ and $CH_3N + H$ dissociations move from 0.06 and 0.01 at the lowest energy to 0.09 and 0.03 at 37.2 kJ/mol up to 0.10 and 0.04 at 65.1 kJ/mol. The absolute rate constants are qualitatively in line with those calculated by Kurosaki et al.[31] The predominance of the $CH_2NH + H$ channel is confirmed, with a rate constant of 4.3×10^{12} s^{-1} (compared to $6.0 \times 10^{12} s^{-1}$ of Kurosaki et al.[31]), while, in our case, the tendency to rearrange to CH_2NH_2 is less than in their calculations (4.3×10^{11} s^{-1} as opposed to 1.6×10^{12} s^{-1} by Kurosaki et al.[31]), leading to a smaller branching ratio for rearrangement. Our diabatic rate constants for dissociation into $CH_3 + NH$ and $CH_3N + H$ are again in line with those of Kurosaki et al.,[31] confirming the small preference for dissociation into $CH_3 + NH$ (reflecting the higher exothermicity of this channel compared to $CH_3N + H$).

In Table 5 can be seen the rate constants for the reactions proceeding from the CH_2NH_2 intermediate. As in the case of the CH_3NH intermediate, the most important of these reactions is dissociation into $CH_2NH + H$ due to the relatively low barrier involved. On the other hand, dissociation into the very endothermic channel, $CH_2 + NH_2(^3B_1)$ is negligible at all energies, reaching a BR of 0.01 at the three highest energies in the diabatic case. Given the high endothermicity of this channel, a low rate constant for its formation is in line with what is expected. Since the only other dissociation of this intermediate, the one into $CHNH_2 + H$, does not present any barriers due to avoided crossings, it can be considered a "loose" transition state. Variational RRKM calculations have been performed at various points along the reaction coordinate and the lowest rate constant obtained has been chosen. Dissociation into $CH_2NH + H$ largely dominates all other channels. The branching ratio for this step remains 0.93−0.92 at all energies. It is followed by rearrangement back into CH_3NH, with a constant branching ratio of 0.05. Finally, dissociation into $CHNH_2 + H$ has a branching ratio of 0.02 at all energies apart from the highest one, 65.1 kJ/mol, where it reaches a value of 0.03. Also in this case, the absolute rate constants are qualitatively in line with Kurosaki et al.,[31] where dissociation into $CH_2NH + H$ is seen to predominate. The rate constant for rearrangement into CH_3NH is more than 1 order of magnitude lower than that of the $CH_2NH + H$ dissociation, whereas the ratio is around 0.5 in the case of Kurosaki et al.[31] Dissociation into $CHNH_2 + H$ and $CH_2(^3B_1) + NH_2$ are confirmed to be minor channels, with the former one being favored. However, our absolute rate constant for the latter channel turns out to be an order of magnitude lower than the one predicted by Kurosaki et al.[31] A probable origin of this is the higher energy associated with this channel in our calculations.

TABLE 6: Global Branching Ratios

	$CH_3N + H$		$CH_2NH + H$		$CH_3 + NH$	
energy (kJ/mol)	A	D	A	D	A	D
0.78		0.01	1	0.92		0.07
1.65		0.01	1	0.92		0.07
2.49		0.01	1	0.92		0.07
22.2		0.02	1	0.90		0.08
29.7		0.02	1	0.90		0.08
37.2		0.03	1	0.89		0.08
46.4		0.03	1	0.88		0.09
65.1		0.04	1	0.86		0.10

In Table 6 are reported the global BR for all reaction channels, obtained by combining rearrangement and dissociation rate constant. The BR for channels (1b), and (1d) are not reported in the Table 6, because once we take into account the rearrangement from the initial intermediate CH_3NH to CH_2NH_2, they become negligibly small.

If we compare the RRKM BR with the experimental determinations, it is clear that both the CH_3N-to-CH_2NH BR determined in the present experiments and the absolute NH yield a room temperature determined by Umemoto et al.[30] are not correctly reproduced by RRKM calculations in none of the approaches used. This is an additional confirmation of the nonstatistical nature of the CH_3NH and CH_2NH_2 dissociation processes, previously suggested by other authors.[29,30,54] In particular, the nascent NH rovibrational distributions have been found to be in line with the formation of an insertion intermediate (CH_3NH), which decomposes before sufficient intramolecular vibrational energy redistribution (IVR) occurs.[29,30,54] Since an efficient IVR is a prerequisite for an RRKM treatment, it is not surprising that RRKM BRs are not in line with the experimental ones. Interestingly, also in the RRKM BRs there is a trend with increasing E_c, which is qualitatively in line with the present experimental determinations.

8. Discussion on the Reaction Mechanism

The reactive scattering results clearly indicate that products of general formula CH_3N are formed through a N/H exchange reaction and that the reaction mechanism is dominated by the formation of one or more bound intermediates. The analysis of the reactive scattering distributions demonstrated that two reactive channels leading to CH_3N isomeric forms are active, the importance of which varies with the total available energy. According to the product energy release, the two contributions can be associated with channel 1a and 1b and 1d. While the attribution of the more exothermic contribution to the $CH_2NH + H$ channel is doubtless, the less exothermic contribution can be consistent with either CH_3N formation or $CHNH_2$, or both. The CM angular distribution associated to channels 1b and 1d is isotropic at all E_c's investigated, while the CM angular distribution associated to channel 1a exhibits an increased preference for forward scattering with increasing collision energy.

Our experimental findings gain support from the characteristics of the calculated NCH_4 PES. According to our calculations, that are at variance with the predictions of Kurosaki et al.,[31] Takayanagi et al.,[32,34] and Jursic,[35] neither the $N(^2D)$ insertion into one of the CH bonds of methane nor the direct H-abstraction are characterized by an energy barrier. The dominance of an insertion reaction mechanism, however, has been invoked to explain previous experimental results. In particular, the nascent NH rovibrational distributions are in line with an insertion mechanism rather than abstraction,[29,30,54] while the large absolute yield associated to the H-displacement channel[30] can only be explained if $N(^2D)$ mostly inserts into a CH bond of methane. An indirect evidence of the dominance of the insertion mechanism comes also from the rate constants measurements[27] and product yields[30] for the reactions with methane isotopomers. Therefore, the insertion mechanism appears to be the dominant one. An explanation for the dominance of the insertion mechanism can be that, even though both insertion and H-abstraction are barrierless at the present level of calculations, the insertion pathway is much more exothermic (leading to the CH_3NH intermediate, stabilized by 445.9 kJ/mol), while the abstraction pathway leading to $NH + CH_3$ products is exothermic by only 126.1 kJ/mol. Notably, the insertion intermediate CH_3NH resides in a potential well that is very deep with respect to the reactants, but not with respect to the very exothermic channel leading to $CH_2NH + H$. In these conditions, it is reasonable to expect that the channel (1a) proceeds through the formation of an osculating complex.[55] A small exit barrier (12.3 kJ/mol with respect to the product asymptote) is present along the minimum energy path and this feature can account for the sizable fraction of energy (0.37−0.42) released as product translational energy.

On the other side, our experimental findings strongly point to a large contribution of another channel leading either to $CH_3N + H$ or to $CHNH_2 + H$, which cannot be reproduced by the statistical RRKM estimates. The characteristics of the second contribution are in line with the observation of an isotropic backward-forward symmetric angular distribution because, due to the reduced exothermicity of both channels 1b and 1c, the system will experience longer the potential energy well associated with the CH_3NH intermediate. We have already commented on the $P(E'_T)$ high energy cutoff, which cannot discriminate with certainty between the two channels. Nevertheless, we note that a large yield of the CH_3N isomer and its increase with collision energy can be adequately explained by dynamical effects. The excess energy released during the formation of the intermediate CH_3NH, in fact, will be concentrated mainly on the two new bonds formed by $N(^2D)$ insertion, that is, N−H and C−N. The fission of one C−H bond—not directly involved in the insertion process—to produce $CH_2NH + H$ requires an efficient energy redistribution, which is not necessary in the case of N−H/C-N bond breaking. In other words, even though the C−H bond is weaker than the newly formed N−H and C−N bonds, the energy released after $N(^2D)$ insertion is so high that there is a significant probability that the stronger N−H or C−N bonds break apart before an efficient IVR occurs. In conclusion, a significant fraction of the CH_3NH intermediates have a lifetime that is long enough for several rotations to occur (so generating a backward-forward symmetric angular distribution), but not long enough for a complete IVR. Other experimental observations relative to channel 1b have suggested that the insertion intermediate that leads to the production of NH is short-lived and decomposes before IVR occurs.[29,30,54] For instance, the substantial similarity of the NH product rovibrational distributions when the reactive partner is a larger alkane (C_2H_6, C_3H_8, $C(CH_3)_4$) has demonstrated that the NH internal states are quite insensitive to the structure of the alkyl radical and are consistent with the formation of a short-lived insertion intermediate.[54] In this view, both $CH_3 + NH$ and $CH_3N + H$ channels become more favored over $CH_2NH + H$ with increasing E_c and total available energy. This is exactly what we have observed in the relative BR between CH_3N and CH_2NH production. Interestingly, Klippenstein[56] has performed some direct dynamics simulations with the forces directly determined from B3LYP/6-31G* evaluations at two energies comparable to those of the

present experiments. According to these calculations, the BR of channel 1c and 1d are much larger than those predictable on statistical grounds and are qualitatively in line with those reported here. The analysis of the trajectories indicates that the increased production of $CH_3N + H$ is related to a correlation between the insertion and dissociation processes and that the average time scale for the H atom loss is quite short (in the range of 50 fs) when CH_3N is formed. If the lifetime of the intermediate is so short, other explanations for the isotropic CM angular distribution are in order. One possibility is that the light atomic hydrogen is frenetically wandering around while leaving the CH_3N cofragment, so that there is not a specific fission direction. An alternative explanation is that the isotropic distribution actually arises from the combination of several direct micromechanisms associated to small and large impact parameters. This explanation appears to be less probable, because the CM angular distribution remains isotropic in the wide range of collision energies investigated. In conclusion, the second contribution derived in our CMB experiments is attributable to the methylnitrene isomer, which is formed in a fast, nonstatistical process. The formation of $CHNH_2$ cannot be ruled out, but no argument, either statistical or dynamic, appears to be in favor of this reaction channel.

A comparison between our data and previous experimental results can be made for the product translational energy release of the H-displacement channels. The average translational energy of ~80 kJ/mol determined by Umemoto et al.[30] corresponds to roughly 22% of the total available energy of the most exothermic channel (1a), that is, quite lower than the fraction we have derived for the lowest E_c experiment. Notably, if we consider our data at E_{c1}, the global average translational energy for channels 1d and 1a (weighted by w_1 and w_2, respectively) is 88.7 kJ/mol. The experiment by Umemoto et al.[30] was performed at room temperature, and therefore, both the relative weights of the two contributions and the details of their $P(E'_T)$'s can be different because of the observed trend with collision energy. Nevertheless, the agreement is such that we can argue that also at room temperature both channels 1d and 1a contribute to the H-displacement mechanism.

8. Implications for the Atmosphere of Titan

We now focus on the role of $N(^2D)$ and reaction 1a in the chemistry of the atmosphere of Titan and on the implications of the present experimental and theoretical results.

The atmosphere of Titan is mainly composed of molecular nitrogen, while the second most abundant molecule is methane.[57,58] In those conditions, it is intuitive that the formation of nitriles (observed in trace amounts) is initiated by some reactions of active forms of nitrogen, such as nitrogen atoms or ions, which can be formed in the upper atmosphere from the dissociation and ionization of the abundant parent molecule N_2. Nitrogen ions are expected to play a significant role in the ionosphere of Titan,[59,60] which has recently revealed a rich chemistry,[61] but below that, since there are practically no radicals that are able to react with undissociated N_2 molecules, a major role in the formation of C−N bonds has to be played by atomic nitrogen. The strong N_2 triple bond (bond energy is 9.76 eV) is extremely difficult to break and, furthermore, there are no optically allowed excitation paths from the ground N_2 electronic state, $X^1\Sigma_g^+$, into repulsive electronically excited states. N_2 dissociation occurs by indirect paths and energetic solar photons can cause N_2 photodissociation via a quite complex mechanism. The absorption of extreme ultraviolet (EUV) radiation by the N_2 molecule, in fact, induces dipole-allowed excitation from the ground *gerade* state to several singlet *ungerade* states that undergo strong predissociation, mainly through the crossing with dissociative triplet states (see for instance refs 62−71). Detailed information about the predissociation probabilities and product state distributions for the excited states of N_2 is therefore fundamental to establish the role of these processes in producing atomic nitrogen in the atmosphere of Earth and other N_2 dominated atmospheres, like that of Titan. At the excitation energies of interest (between 100 000 cm^{-1} and the first ionization limit of 125 666 cm^{-1}) molecular nitrogen exhibits a complex and congested spectrum and the predissociation mechanisms are not well characterized. Because of the different reactivity of ground ^4S and excited ^2D atomic nitrogen and the long radiative lifetime of the excited state, it is quite important to characterize the N_2 predissociation yield to quantify the relative concentration of the two states and their role in the atmospheric chemistry of Titan. Unfortunately, the $N(^2D)$ and $N(^4S)$ production yields have been measured only for few specific rovibrational of several electronic states of N_2 by Walter et al.[71] and Helm and Cosby.[72] The observations are therefore sparse and do not allow us to derive a general model that can describe quantitatively the predissociation products of N_2. Neverthelss, even though the few states investigated cannot alone account for the complex phenomenology occurring in the upper atmospheres of Earth and Titan, some observations of the authors can help in drawing more general conclusions. They have observed that the predissociation of the above-mentioned levels always produces one ground state atom and one excited atom, in either the ^2D or ^2P states. The energetic limit of the $N(^2D) + N(^2D)$ channel is quite high and it was never observed in the above-mentioned experiments. Remarkably, no dissociation was observed to ground state $N(^4S) + N(^4S)$. With the limited experimental information available, probably the best scheme is the one recently suggested by Bakalian[73] in modeling the production of hot nitrogen atoms in the martian thermosphere. According to it, the N_2 photodissociation proceeds along three possible channels:

$$N_2 + h\nu \rightarrow N(^4S) + N(^4S) \quad (2a)$$

$$N_2 + h\nu \rightarrow N(^4S) + N(^2D) \quad (2b)$$

$$N_2 + h\nu \rightarrow N(^4S) + N(^2P) \quad (2c)$$

where the threshold dissociation energies are 9.76, 12.14, and 13.33 eV, respectively, for channels 2a, 2b, and 2c. For photon energies between 9.76 and 12.14 eV, photodissociation (if it occurs at all) has been taken to proceed along channel 2a, the only accessible channel at these energies. For photon energies between 12.14 eV, the threshold dissociation energy for channel 2b, and 14.0346 eV, the upper absorption limit observed for this channel,[71] the photodissociation proceeds through channel 2b, while at photon energies between 13.886 and 14.52 eV it can proceed along channel 2c. At photon energies greater than 14.52 eV, the photodissociation of N_2 proceeds along the $N(^4S) + N(^2D)$ and $N(^4S) + N(^2P)$ pathways. Since the ^2P state rapidly decays to the ^2D state, in the modeling of the atmosphere of Titan this approach is not expected to produce results significantly different from those obtained by simply assuming that N_2 dissociation produces one nitrogen atom in the ground ^4S state and one atom in the ^2D state. This choice has been made in the models by Wilson and Atreya,[23] Lavvas et al.,[24] and

Strobel.[74] Less realistic appears to be the assumption that two $N(^2D)$ atoms are produced, as done in the models by Toublanc et al.,[20] Lara et al.,[21] and Lebonnois et al.[22] We recall that in the model of Yung et al.[19] the photodissociation of N_2 was not included at all.

In addition to EUV photodissociation, in the upper atmosphere of Titan N_2 molecules are subject to significant bombardment both by energetic (200 eV) magnetospheric electrons and by lower energy electrons produced by photoionization processes. Since the energy involved is high, electron impact can induce ionization, dissociative ionization, excitation and dissociation. It has been widely demonstrated,[75,76] that the N_2 electron impact excitation followed by dissociation gives essentially the same results as those induced by EUV photon absorption. This is not surprising because the N_2 singlet state levels populated by optical absorption or electron impact excitation of the ground $X^1\Sigma_g^+$ state are the same and their lifetimes are so long that their formation (excitation) and decay (fluorescence and predissociation) can be considered independent processes.[75,76] The electron impact dissociation of N_2 has been characterized in a crossed beam experiment at electron energies between 18.5 and 148.5 eV. The observed translational energy release was consistent with the formation of $N(^2D) + N(^4S)$, which can therefore be considered the primary dissociation channel. $N(^4S) + N(^4S)$ and $N(^2P) + N(^4S)$ channel were considered to give only a small contribution, outside the sensitivity of the experimental method.

In conclusion, the two main processes leading to the breakup of N_2 molecules in the upper atmosphere of Titan equally produce $N(^4S)$ and $N(^2D)$. In addition to them, nitrogen atoms in the ^2D state can also be formed in the electron impact dissociative ionization process

$$N_2 + e^- \rightarrow N(^2D) + N^+ + 2e^- \quad (3)$$

when using high electron energies, and the channel leading to $N(^2D) + N^+(^3P)$ has been found to be the main one in dissociative photoionization of N_2 at photon energies higher than 26.55 eV.[77]

In addition, $N(^2D)$ can be formed by N_2^+ dissociation recombination. All the observed channels produce one or more nitrogen atoms in the ^2D or ^2P state

$$N_2^+ + e^- \rightarrow N(^4S) + N(^2D) \quad (4a)$$

$$N_2^+ + e^- \rightarrow N(^4S) + N(^2P) \quad (4b)$$

$$N_2^+ + e^- \rightarrow N(^2D) + N(^2D) \quad (4c)$$

where the experimental BR for channels 4a, 4b, and 4c have been determined to be, respectively, 0.37, 0.11, and 0.54 by Peterson et al.[78] and 0.46, 0.08, and 0.46 by Kella et al.[79]

Finally, penetrating galactic cosmic rays have also been considered a potential source of energy down to the lower atmosphere of Titan: the cosmic ray spectrum is such that a large fraction of the total energy flux is carried by particles (mostly protons, with 10−15% α particles and heavier nuclei) with kinetic energies in excess of 1 GeV. The absorption of these high-energy particles will produce electromagnetic and particle cascades that can dissociate N_2 in the lower atmosphere of Titan. Even though the modeling of the interaction between the galactic cosmic rays and the most abundant component of the atmosphere of Titan N_2 is quite complex, the net result has been predicted to be dissociation, excitation, ionization, and dissociative ionization.[80] All these processes then contribute to the generation of $N(^2D)$ similarly to what seen previously.

After settling the $N(^2D)$ formation routes in the upper atmosphere of Titan, we now turn our attention to the role of reaction 1a. Since the first photochemical model by Yung et al.,[19] reaction 1a has been recognized to be an important one, because of the relatively large abundance of methane and the small rate constant associated to the collisional deactivation of $N(^2D)$ by N_2 (the room temperature recommended value[14] is $k = 1.7 \times 10^{-14}$ cm^3 molecule^{-1} s^{-1}). Reaction 1a was included in the model of Yung et al.[19] with the rate constant value of 3×10^{-12} cm^3 molecule^{-1} s^{-1} determined at room temperature by Black et al.[25] Since the main products were unknown until recently, they were assumed to be $NH + CH_3$ so that the $N(^2D) + CH_4 \rightarrow NH + CH_3$ reaction was at the same time the main mechanism of NH formation (thus determining the odd nitrogen budget of the atmosphere), and the main mechanism of CH_3 formation (that because, erroneously, the photolysis of methane was not considered to produce directly CH_3 at that time). In addition, the $N(^2D) + CH_4 \rightarrow NH + CH_3$ reaction was considered an important step toward the formation of HCN in a complex scheme involving five elementary reactions (scheme 2 in Yung et al.[19]). In the more recent photochemical models of Toublanc et al.[20] and of Lara et al.[21] the reaction $N(^2D) + CH_4$ was maintained with the same value of the rate constant and with the same reaction products. In any case, the importance of the $N(^2D) + CH_4 \rightarrow NH + CH_3$ reaction was diminished in the models developed after that of Yung et al., as other HCN formation mechanisms were envisaged and an alternative photolysis scheme of CH_4 introduced. In the most recent models of Wilson and Atreya[23] and Lavvas et al.[24] the more recent rate constant values determined by Umemoto et al.[27] and Takayanagi et al.[28] are referred to and the absolute yield of NH and H determined by Umemoto et al.[30] introduced, with the assumption that H is produced exclusively in conjunction with CH_2NH.

In view of the present and previous detailed experimental results, a fairly complete characterization of the reaction 1a is now available. The most important implications are here summarized.

The early assumption that only $NH + CH_3$ are the products of the $N(^2D) + CH_4$ reaction is not correct: that reactive channel accounts only for about 30% in the room temperature laboratory experiment and, by analyzing the trend of the BR as a function of the available energy for the dynamically similar $CH_3N + H$ channel, we can presume that it will be even minor under the low temperature conditions of Titan's atmosphere. Unfortunately, since this reactive system deviates remarkably from statistical behavior, we cannot refer to our RRKM calculations performed at the energy of relevance to the atmosphere of Titan to evaluate the product BRs. Furthermore, even though they are performed at collision energies higher than those achievable at the low temperature typical of the atmosphere of Titan, the present crossed molecular beam results confirm that the reaction $N(^2D) + CH_4$ is an active route of formation of methanimine, a closed-shell molecule containing a novel C−N bond. That demonstrates that such a bond can be generated directly by a reaction involving an active form of N_2, the main constituent of the atmosphere of Titan, and CH_4, the second most abundant species. CH_2NH has not been observed directly in Titan's atmosphere so far, but its protonated form, $CH_2NH_2^+$, has been invoked to reproduce the peak at $m/z = 30$ recorded by the ion

neutral mass spectrometer (INMS) on the Cassini spacecraft.[81] The presence of a double CN bond renders CH_2NH a very reactive molecule, and similarly to the entire family of imines, methanimine easily undergoes polymerization, oxidation, and hydrolysis. The characterization of this transient species in the laboratory has been possible only by producing it in situ from the pyrolysis of amines, methyl azide and other azido compounds.[82,83] Therefore, it is reasonable to assume that in a relatively dense medium such as the upper atmosphere of Titan, methanimine quickly reacts with radicals or undergoes polymerization and copolymerization. Alternatively, it could photodissociate to HCNH/CH_2NH + H or HCN/HNC + H_2. The absorption cross section of CH_2NH has been measured in the 235−260 nm range,[82] but the photodissociation product yield has not been characterized. Nevertheless, it is known that CH_2NH can dissociate[48c,83] to HCNH/CH_2NH + H or HCN/HNC + H_2 along the ground state PES via quite large energy barriers,[48c] which can certainly be overcome after UV absorption to an excited state and internal conversion to the ground electronic state. In conclusion, an efficient HCN formation route can be envisaged on the basis of the sequence

$$N(^2D) + CH_4 \rightarrow CH_2NH + H \quad (1a)$$

$$CH_2NH + h\nu \rightarrow HCN + H_2 \quad (5a)$$

$$CH_2NH + h\nu \rightarrow H_2CN + H \quad (5b)$$

$$H_2CN + H \rightarrow HCN + H_2 \quad (6)$$

This HCN formation sequence could be as efficient as other routes already included, such as that based on the reaction $N(^4S)$ + CH_3, which involves ground state nitrogen atoms but requires a reactive encounter between two radicals, a relatively rare event in a dense medium such as the atmosphere of Titan.

Interestingly, most of the above-mentioned processes have been included in the very recent photochemical model of Titan by Lavvas et al.,[24] who were the first to consider the possible transformation that CH_2NH undergoes after its formation. Because of the lack of experimental parameters, the effect of some processes, such as the formation of CH_2NH dimer or the copolymerization with other nitriles, could only be estimated. Nevertheless, several interesting considerations have been made. For instance, if the main photolysis product is assumed to be the H_2CN radical rather than HCN, there are no significant changes in the HCN profile, since the H_2CN is readily converted to HCN by reaction with H. As a matter of fact, the model by Lavvas et al.[24] appears to predict a larger quantity of CH_2NH than necessary to reproduce the INMS observation, so implying that there is an overestimate of CH_2NH production or an underestimate of CH_2NH loss. In this respect, the use of the present experimental results could be of help, as Lavvas et al.[24] have used for channel 1a a yield of 0.8 in accord with the suggestion of Umemoto et al.,[30] while also methylnitrene is formed. They have also used the rate constant temperature dependence derived in a T range that does not comprise the range of temperatures typical of the atmosphere of Titan. Other $k(T)$ measurements at the relevant temperature are in order. Finally, laboratory measurements of CH_2NH photoabsorption cross section in a wider range of wavelengths and photoproducts yields, as well as the determination of the rate constants for CH_2NH reactions with species (including ions) abundant in the atmosphere of Titan, can help to understand the role of this species in the nitrile chemistry of Titan. Other desiderata include the experimental investigation of CH_2NH polymerization and copolymerization with other N-containing species. In this respect, it is interesting to note that the model by Lavvas et al.[24] has confirmed an important contribution of nitriles chemistry in the formation of Titan's haze, the analysis of which by the aerosol collector and pyrolyser during the Huygens probe descent revealed a large content of nitrogen.[84]

9. Conclusion

In summary, we have investigated the H-displacement dynamics of the reactions $N(^2D)$ + CH_4 at different collision energies by the CMB method complemented by ab initio and RRKM calculations. The CMB results have identified two distinct isomers as primary reaction products, methanimine and methylnitrene, the yield of which significantly varies with the total available energy. From the derived CM product angular and translational energy distributions the reaction micromechanisms, the product energy partitioning and the relative branching ratios of the competing reaction channels leading to the two isomers have been obtained. Differently from previous theoretical studies, both insertion and H-abstraction pathways have been found to be barrierless at all levels of theory employed in the present calculations. The comparison with RRKM predictions of the relative branching ratio confirms the highly nonstatistical nature of the $N(^2D)$ + CH_4 reaction, with the production of the CH_3N isomer dominated by dynamical effects. The implications for the chemical models of the atmosphere of Titan, and possibly of objects where both N_2 and methane are present, such as Triton and Pluto, have been discussed.

Acknowledgment. We acknowledge financial support from the Italian MIUR (Ministero Istruzione Università Ricerca) under projects PRIN (2007H9S8SW_004 and 2007WLBXX9_004) and European Commission through the Coordination Action 001637 (Europlanet). This work is also supported by the European Union Marie-Curie human resources and mobility programme under contract MCRTN-CT-2004-512302 (Molecular Universe). M.R. thanks Peter R. Schreiner for helpful discussions. D.S. thanks Alexander Mebel for useful suggestions on RRKM calculations.

Supporting Information Available: Total energies, the geometrical parameters, and the vibrational frequencies of all the stationary points (minima and saddle points). This material is available free of charge via the Internet at http://pubs.acs.org.

References and Notes

(1) Chemical Kinetics and Photochemical Data for Use in Atmospheric Studies. Evaluation No. 15; JPL Publication 06-2, Jet Propulsion Laboratory: Pasadena, CA, 2006.

(2) Yung, Y. L.; DeMore, W. B. *Photochemistry of Planetary Atmospheres*; Oxford University Press: New York, 1998.

(3) Van Regemorter, T.; Larsson, K. *Phys. Chem. A* **2009**, *113*, 3274. Shah, Z. M.; Mainwood, A. *Diam. Relat. Mater.* **2008**, *17*, 1307. Kshirsagar, S. T.; Kshirsagar, R. B.; Patil, P. S.; Kulkarni, A.; Mandate, A. B.; Gaikwad, A. B.; Gokhale, S. P. *Diam. Relat. Mater.* **2005**, *14*, 232. Smith, J. A.; Wills, J. B.; Moores, H. S.; Orr-Ewing, A. J.; Ashfold, M. N. R.; Mankelevich, Y. A.; Suetin, N. V. *J. Appl. Phys.* **2002**, *92*, 672. Mankelevich, Y. A.; Suetin, N. V.; Smith, J. A.; Ashfold, M. N. R. *Diam. Relat. Mater.* **2002**, *11*, 567. Smith, J. A.; Rosser, K. N.; Yagi, H.; Wallace, M. I.; May, P. W.; Ashfold, M. N. R. *Diam. Relat. Mater.* **2001**, *10*, 370.

(4) Pintassilgo, C. D.; Jaoul, C.; Loureiro, J.; Belmonte, T.; Czerwiec, T. *J. Phys. D-Appl. Phys.* **2007**, *40*, 3620.

(5) Baulch, D. L.; Bowman, C. T.; Cobos, C. J.; Cox, R. A.; Just, T.; Kerr, J. A.; Pilling, M. J.; Stocker, D.; Troe, J.; Tsang, W.; Walker, R. W.; Warnatz, J. *J. Phys. Chem. Ref. Data* **2005**, *34*, 757.

(6) Alagia, M.; Aquilanti, V.; Ascenzi, D.; Balucani, N.; Cappelletti, D.; Cartechini, L.; Casavecchia, P.; Pirani, F.; Sanchini, G.; Volpi, G. G. *Isr. J. Chem.* **1997**, *37*, 329.

(7) Balucani, N.; Alagia, M.; Cartechini, L.; Casavecchia, P.; Volpi, G. G.; Sato, K.; Takayanagi, T.; Kurosaki, Y. *J. Am. Chem. Soc.* **2000**, *122*, 4443.

(8) Balucani, N.; Cartechini, L.; Alagia, M.; Casavecchia, P.; Volpi, G. G. *J. Phys. Chem. A* **2000**, *104*, 5655.

(9) Casavecchia, P.; Balucani, N.; Cartechini, L.; Capozza, G.; Bergeat, A.; Volpi, G. G. *Faraday Discuss.* **2001**, *119*, 27.

(10) Balucani, N.; Casavecchia, P.; Banares, L.; Aoiz, F. J.; Gonzalez-Lezana, T.; Honvault, P.; Launay, J. M. *J. Phys. Chem. A* **2006**, *110*, 817. Balucani, N.; Cartechini, L.; Capozza, G.; Segoloni, E.; Casavecchia, P.; Volpi, G. G.; Aoiz, F. J.; Bañares, L.; Honvault, P.; Launay, J.-M. *Phys. Rev. Lett.* **2002**, *89*, 013201.

(11) Alagia, M.; Balucani, N.; Cartechini, L.; Casavecchia, P.; Volpi, G. G.; Pederson, L. A.; Schatz, G. C.; Lendvay, G.; Harding, L. B.; Hollebek, T.; Ho, T.-S.; Rabitz, H. *J. Chem. Phys.* **1999**, *110*, 8857. Balucani, N.; Alagia, M.; Cartechini, L.; Casavecchia, P.; Volpi, G. G.; Pederson, L. A.; Schatz, G. C. *J. Phys. Chem. A* **2001**, *105*, 2414.

(12) Balucani, N.; Casavecchia, P. *Orig. Life Evol. Biosph.* **2006**, *36*, 443.

(13) Schofield, K. *J. Phys. Chem. Ref. Data* **1979**, *8*, 723.

(14) Herron, J. T. *J. Phys. Chem. Ref. Data* **1999**, *28*, 1453.

(15) Bertrand, C.; van Tiggelen, P. J. *J. Phys. Chem.* **1974**, *78*, 2320. Guillaume, P.; François, C.; van Tiggelen, P. J. *Bull. Soc. Chim. Belg.* **1983**, *92*, 633.

(16) Schmatjko, K. J.; Wolfrum, J. *Ber. Bunsen-Ges. Phys. Chem.* **1978**, *82*, 419.

(17) Miller, J. A.; Bowman, C. T. *Prog. Energy Combust. Sci.* **1989**, *15*, 287.

(18) Manaa, M. R.; Yarkony, D. R. *Chem. Phys. Lett.* **1992**, *188*, 352.

(19) Yung, Y.; Allen, M.; Pinto, J. *Astrophys. J. Suppl. Ser.* **1984**, *55*, 465.

(20) Toublanc, D.; Parisot, J.; Brillet, J.; Gautier, D.; Raulin, F.; McKay, C. *Icarus* **1995**, *113*, 2.

(21) Lara, L. M.; Lellouch, E.; López-Moreno, J. J.; Rodrigo, R. *J. Geophys. Res.* **1996**, *101*, 23261.

(22) Lebonnois, S.; Toublanc, D.; Hourdin, F.; Rannou, P. *Icarus* **2001**, *152*, 384.

(23) Wilson, E. H.; Atreya, S. *J. Geophys. Res.* **2004**, *109*, E06002.

(24) Lavvas, P. P.; Coustenis, A.; Vardavas, I. M. *Planet. Space Sci.* **2008**, *56*, 27. Lavvas, P. P.; Coustenis, A.; Vardavas, I. M. *Planet. Space Sci.* **2008**, *56*, 67.

(25) Black, G.; Slanger, T. G.; St. John, G. A.; Young, R. A. *J. Chem. Phys.* **1969**, *51*, 116.

(26) Fell, B.; Rivas, I. V.; McFadden, D. L. *J. Phys. Chem.* **1981**, *85*, 224.

(27) Umemoto, H.; Hachiya, N.; Matsunaga, E.; Suda, A.; Kawasaki, M. *Chem. Phys. Lett.* **1998**, *296*, 203.

(28) Takayanagi, T.; Kurosaki, Y.; Sato, K.; Misawa, K.; Kobayashi, Y.; Tsunashima, S. *J. Phys. Chem. A* **1999**, *103*, 250.

(29) Umemoto, H.; Kimura, Y.; Asai, T. *Chem. Phys. Lett.* **1997**, *264*, 215.

(30) Umemoto, H.; Nakae, T.; Hashimoto, H.; Kongo, K.; Kawasaki, M. *J. Chem. Phys.* **1998**, *109*, 5844.

(31) Kurosaki, Y.; Takayanagi, T.; Sato, K.; Tsunashima, S. *J. Phys. Chem. A* **1998**, *102*, 254.

(32) Takayanagi, T.; Kurosaki, Y.; Yokoyama, K. *Int. J. Quantum Chem.* **2000**, *79*, 190.

(33) Jursic, B. S. *Int. J. Quantum Chem.* **1999**, *71*, 481.

(34) Takayanagi, T.; Kurosaki, Y. *J. Mol. Struct. (THEOCHEM)* **1999**, *492*, 151.

(35) Balucani, N. *Int. J. Mol. Sci.* **2009**, *10*, 2304.

(36) Alagia, M.; Balucani, N.; Casavecchia, P.; Stranges, D.; Volpi, G. G. *J. Chem. Soc., Faraday Trans.* **1995**, *91*, 575.

(37) Balucani, N.; Capozza, G.; Leonori, F.; Segoloni, E.; Casavecchia, P. *Int. Rev. Phys. Chem.* **2006**, *25*, 109.

(38) Herron, J. T.; Huie, R. E. *J. Phys. Chem.* **1968**, *72*, 2538.

(39) Umemoto, H.; Sugiyama, K.; Tsunashima, S.; Sato, S. S. *Bull. Chem. Soc. Jpn.* **1985**, *58*, 3076.

(40) (a) Becke, A. D. *J. Phys. Chem.* **1993**, *98*, 5648. (b) Stephens, P. J.; Devlin, F. J.; Chablowski, C. F.; Frisch, M. J. *J. Phys. Chem.* **1994**, *98*, 11623.

(41) (a) Dunning, T. H., Jr. *J. Chem. Phys.* **1989**, *90*, 1007. (b) Woon, D. E.; Dunning, T. H., Jr. *J. Chem. Phys.* **1993**, *98*, 1358. (c) Kendall, R. A.; Dunning, T. H., Jr.; Harrison, R. J. *J. Chem. Phys.* **1992**, *96*, 6796.

(42) (a) Gonzales, C.; Schlegel, H. B. *J. Chem. Phys.* **1989**, *90*, 2154. (b) *J. Phys. Chem.* **1990**, *94*, 5523.

(43) (a) Bartlett, R. J. *Annu. Rev. Phys. Chem.* **1981**, *32*, 359. (b) Raghavachari, K.; Trucks, G. W.; Pople, J. A.; Head-Gordon, M. *Chem. Phys. Lett.* **1989**, *157*, 479. (c) Olsen, J.; Jorgensen, P.; Koch, H.; Balkova, A.; Bartlett, R. J. *J. Chem. Phys.* **1996**, *104*, 8007.

(44) (a) Martin, J. M. L.; de Oliveira, G. *J. Chem. Phys.* **1999**, *111*, 1843. (b) Parthiban, S.; Martin, J. M. L. *J. Chem. Phys.* **2001**, *114*, 6014.

(45) Frisch, M. J.; Trucks, G. W.; Schlegel, H. B.; Scuseria, G. E.; Robb, M. A.; Cheeseman, J. R.; Montgomery, J. A., Jr.; Vreven, T.; Kudin, K. N.; Burant, J. C.; Millam, J. M.; Iyengar, S. S.; Tomasi, J.; Barone, V.; Mennucci, B.; Cossi, M.; Scalmani, G.; Rega, N.; Petersson, G. A.; Nakatsuji, H.; Hada, M.; Ehara, M.; Toyota, K.; Fukuda, R.; Hasegawa, J.; Ishida, M. Nakajima, T.; Honda, Y.; Kitao, O.; Nakai, H.; Klene, M. Li, X.; Knox, J. E. ; Hratchian, H. P.; Cross, J. B.; Bakken, V.; Adamo, C.; Jaramillo, J.; Gomperts, R.; Stratmann, R. E.; Yazyev, O.; Austin, A. J.; Cammi, R.; Pomelli, C.; Ochterski, J. W.; Ayala, P. Y.; Morokuma, K.; Voth, G. A.; Salvador, P.; Dannenberg, J. J.; Zakrzewski, V. G.; Dapprich, S.; Daniels, A. D.; Strain, M. C.; Farkas, O.; Malick, D. K.; Rabuck, A. D.; Raghavachari, K.; Foresman, J. B.; Ortiz, J. V.; Cui, Q.; Baboul, A. G.; Clifford, S.; Cioslowski, J.; Stefanov, B. B.; Liu, G.; Liashenko, A.; Piskorz, P.; Komaromi, I.; Martin, R. L.; Fox, D. J.; Keith, T.; Al-Laham, M. A.; Peng, C. Y.; Nanayakkara, A.; Challacombe, M.; Gill, P. M. W.; Johnson, B.; Chen, W.; Wong, M. W.; Gonzalez, C.; Pople, J. A. *Gaussian 03*, Revision D.01; Gaussian, Inc.: Wallingford, CT, 2004.

(46) (a) *MOLEKEL 4.3*, Flükiger, P.; Lüthi, H. P.; Portmann, S.; Weber, J. Swiss Center for Scientific Computing, Manno (Switzerland), 2000−2002. (b) Portmann, S.; Lüthi, H. P. *Chimia* **2000**, *54*, 766.

(47) Gilbert, R. G.; Smith, S. C. *Theory of unimolecular and recombination reactions*; Blackwell Scientific Publications: Cambridge, U.K., 1990.

(48) (a) Xie, Y.; Scuseria, G. E.; Yates, B. F.; Yamaguchi, Y.; Schaefer, H. F., III. *J. Amer. Chem. Soc.* **1989**, *111*, 5181. (b) Arenas, J. F.; Marcos, J. I.; Otero, J. C.; Sánchez-Gálvez, A.; Soto, J. *J. Chem. Phys.* **1999**, *111*, 551. (c) Nguyen, M. T.; Sengupta, D.; Ha, T.-K. *J. Phys. Chem.* **1996**, *110*, 6499. (d) Hou, C.-Y.; Zhang, H.-X.; Sun, C.-c. *J. Phys. Chem. A* **2006**, *110*, 10260.

(49) De Oliveira, G.; Martin, J. M. L.; Silwan, I. K. C.; Liebman, J. F. *J. Comput. Chem.* **2001**, *13*, 1297.

(50) (a) Fokin, A. A.; Shubina, T. E.; Gunchenko, P. A.; Isaev, S. D.; Yurchenko, A. G.; Schreiner, P. R. *J. Am. Chem. Soc.* **2002**, *124*, 10718. (b) Schreiner, P.; Fokin, A. A.; Schleyer, P. v. R.; Schaefer, H. F., III. In *Fundamental World of Quantum Chemistry*; Bründas, E. J., Kryachko, E. S., Eds.; Kluwer: The Netherlands, 2003; Vol. II, pp 349−375.

(51) Travers, M. J.; Cowles, D. C.; Clifford, E. P.; Ellison, G. B. *J. Chem. Phys.* **1999**, *111*, 5349.

(52) Richards, C., Jr.; Meredith, C.; Kim, S.-J.; Quelch, G. E.; Schaefer, H. F., III. *J. Chem. Phys.* **1994**, *100*, 481.

(53) Marcy, T. P.; Diaz, R. R.; Heard, D.; Leone, S. R.; Harding, L. B.; Klippenstein, S. J. *J. Phys. Chem. A* **2001**, *105*, 8361.

(54) Umemoto, H.; Kimura, Y.; Asai, T. *Bull. Chem. Soc. Jpn.* **1997**, *70*, 2951.

(55) Fisk, G. A.; McDonald, J. D.; Herschbach, D. R. *Discuss. Faraday Soc.* **1967**, *44*, 228.

(56) Klippenstein, S. J. *Faraday Discuss.* **2001**, *119*, 121.

(57) Niemann, H. B.; Atreya, S. K.; Bauer, S. J.; Carignan, G. R.; Demick, J. E.; Frost, R. L.; Gautier, D.; Haberman, J. A.; Harpold, D. N.; Hunten, D. M.; Israel, G.; Lunine, J. I.; Kasprzak, W. T.; Owen, T. C.; Paulkovich, M.; Raulin, F.; Raaen, E.; Way, S. H. *Nature* **2005**, *438*, 779.

(58) Coustenis, A.; Salama, A.; Schulz, B.; Ott, S.; Lellouch, E.; Encrenaz, T.; Gautier, D.; Feuchtgruber, H. *Icarus* **2003**, *161*, 383.

(59) Vuitton, V.; Yelle, R. V.; McEwan, M. J. *Icarus* **2007**, *191*, 722.

(60) Carrasco, N.; Alcaraz, C.; Dutuit, O.; Plessis, S.; Thissen, R.; Vuitton, V.; Yelle, R.; Pernot, P. *Planet. Space Sci.* **2008**, *56*, 1644.

(61) Cravens, T. E.; Robertson, I. P.; Waite, J. H.; Yelle, R. V.; Kasprzak, W. T.; Keller, C. N.; Ledvina, S. A.; Niemann, H. B.; Luhmann, J. G.; McNutt, R. L.; Ip, W. H.; De La Haye, V.; Mueller-Wodarg, I.; Wahlund, J. E.; Anicich, V. G.; Vuitton, V. *Geophys. Res. Lett.* **2006**, *33*, L07105.

(62) Beyer, K. D.; Welge, K. H. *J. Chem. Phys.* **1969**, *51*, 5323.

(63) Buijsse, B.; van der Zande, W. J. *Faraday Discuss.* **1997**, *108*, 271.

(64) Helm, H.; Cosby, P. C. *J. Chem. Phys.* **1989**, *90*, 4208.

(65) Lewis, B. R.; Gibson, S. T.; Sprengers, J. P.; Ubachs, W.; Johansson, A.; Wahlström, C.-G. *J. Chem. Phys.* **2005**, *123*, 236101.

(66) Sprengers, J. P.; Ubachs, W.; Baldwin, K. G. H.; Lewis, B. R.; Tchang-Brillet, W.-U. *J. Chem. Phys.* **2003**, *119*, 3160.

(67) Sprengers, J. P.; Ubachs, W.; Johansson, A.; L'Huillier, A.; Wahlstrom, C.-G.; Lang, R.; Lewis, B. R.; Gibson, S. T. *J. Chem. Phys.* **2004**, *120*, 8973.

(68) Sprengers, J. P.; Reinhold, E.; Ubachs, W.; Baldwin, K. G. H.; Lewis, B. R. *J. Chem. Phys.* **2005**, *123*, 144315.

(69) Sprengers, J. P.; Ubachs, W.; Baldwin, K. G. H. *J. Chem. Phys.* **2005**, *122*, 144301.

(70) Ubachs, W.; Velchev, I.; de Lange, A. *J. Chem. Phys.* **2000**, *112*, 5711.

(71) Walter, C. W.; Cosby, P. C.; Helm, H. *J. Chem. Phys.* **1993**, *99*, 3553.

(72) Helm, H.; Cosby, P. C. *J. Chem. Phys.* **1989**, *90*, 4208.

(73) Bakalian, F. *Icarus* **2006**, *183*, 69.

(74) Strobel, D. F. *Space Sci. Rev.* **2005**, *116*, 155.
(75) Cosby, P. C. *J. Chem. Phys.* **1993**, *98*, 9544.
(76) Zipf, E. C.; McLaughlin, R. W. *Planet. Space Sci.* **1978**, *26*, 449.
(77) Nicolas, C.; Alcaraz, C.; Thissen, R.; Vervloet, M.; Dutuit, O. *J. Phys. B: At. Mol. Phys.* **2003**, *36*, 2239.
(78) Peterson, K. J. R.; Le Padellec, A.; Danared, H.; Dunn, G. H.; Larsson, M.; Larson, A.; Peverall, R.; Stromholm, C.; Rosen, S.; af Ugglas, M.; van der Zande, W. J. *J. Chem. Phys.* **1998**, *108*, 1978.
(79) Kella, D.; Johnson, P. J.; Pedersen, H. B.; Vejby-Christensen, L.; Andersen, L. H. *Phys. Rev. Lett.* **1996**, *77*, 2432–2435.
(80) Molina-Cuberosa, G. J.; Lopez-Moreno, J. J.; Rodrigo, R.; Larab, L. M.; O'Brien, K. *Planet. Space Sci.* **1999**, *47*, 1347.
(81) Vuitton, V.; Yelle, R. V.; Anicich, V. G. *Astrophys. J.* **2006**, *647*, L175–L178.
(82) Teslja, A.; Nizamov, B.; Dagdigian, P. J. *J. Phys. Chem. A* **2004**, *108*, 4433.
(83) Larson, C.; Ji, Y. Y.; Samartzis, P.; Wodtke, A. M.; Lee, S. H.; Lin, J. J. M.; Chaudhuri, C.; Ching, T. T. *J. Chem. Phys.* **2006**, *125*, 133302.
(84) Israel, G.; Szopa, C.; Raulin, F.; Cabane, M.; Niemann, H. B.; Atreya, S. K.; Bauer, S. J.; Brun, J. F.; Chassefiere, E.; Coll, P.; Conde, E.; Coscia, D.; Hauchecorne, A.; Millian, P.; Nguyen, M. J.; Owen, T.; Riedler, W.; Samuelson, R. E.; Siguier, J. M.; Steller, M.; Sternberg, R.; Vidal-Madjar, C. *Nature* **2005**, *438*, 796.

JP904302G